PHYSICAL REVIEW B **94**, 180403(R) (2016)

Anisotropic Hanle line shape via magnetothermoelectric phenomena

K. S. Das,[1,*] F. K. Dejene,[2] B. J. van Wees,[1] and I. J. Vera-Marun[1,3,†]

[1]*Zernike Institute for Advanced Materials, University of Groningen, 9747 AG Groningen, The Netherlands*

[2]*Max Planck Institute of Microstructure Physics, D-06120 Halle, Germany*

[3]*School of Physics and Astronomy, University of Manchester, Manchester M13 9PL, United Kingdom*

(Received 2 April 2016; revised manuscript received 5 August 2016; published 7 November 2016)

We observe anisotropic Hanle line shape with unequal in-plane and out-of-plane nonlocal signals for spin precession measurements carried out on lateral metallic spin valves with transparent interfaces. The conventional interpretation for this anisotropy corresponds to unequal spin relaxation times for in-plane and out-of-plane spin orientations as for the case of two-dimensional materials like graphene, but it is unexpected in a polycrystalline metallic channel. Systematic measurements as a function of temperature and channel length, combined with both analytical and numerical thermoelectric transport models, demonstrate that the anisotropy in the Hanle line shape is magnetothermal in origin, caused by the anisotropic modulation of the Peltier and Seebeck coefficients of the ferromagnetic electrodes. Our results call for the consideration of such magnetothermoelectric effects in the study of anisotropic spin relaxation.

DOI: 10.1103/PhysRevB.94.180403

Electrical spin injection and detection in nonlocal lateral spin valves have been used extensively to study pure spin currents in nonmagnetic (NM) materials [1–8]. Hanle measurements allow the manipulation of the spin accumulation in the NM materials via a perpendicular magnetic field, which induces spin precession as the carriers diffuse along the NM channel. From these experiments, we can extract the spin transport parameters of the channel, like the spin relaxation length and time, and hence get an insight into the nature of spin-orbit interaction (SOI) causing spin relaxation. This is particularly relevant for two-dimensional materials like graphene, where the SOI acting along the in-plane and out-of-the plane directions can differ and lead to anisotropic spin relaxation, manifested by different signals for the in-plane and out-of-plane spin configurations in the Hanle experiments [9,10]. In contrast, for polycrystalline films, spin relaxation is expected to be isotropic [11].

In this work we use metallic nonlocal spin valves (NLSVs), with aluminium (Al) as the NM material, to study spin precession as a function of temperature. Permalloy ($Ni_{80}Fe_{20}$, Py) has been used as the ferromagnetic (FM) electrodes to inject a spin-polarized current into Al across a transparent interface and to nonlocally detect the nonequilibrium spin accumulation in Al at a distance L from the injector. This model system with transparent FM/NM interfaces has been thoroughly studied via spin valve measurements. But curiously, corresponding spin precession studies in such systems are scarce. Only recently a few groups have demonstrated spin precession in NLSVs with transparent FM/NM interfaces [12,13], with the NM channel being either silver or copper. More importantly, these few experiments have been done only at low temperatures ($T \leqslant 10$ K), with no reports on Hanle measurements at room temperature for transparent FM/NM interfaces.

We demonstrate, through nonlocal spin precession experiments on Py/Al NLSVs with transparent interfaces, an anomalous Hanle line shape for $T > 150$ K, in which the in-plane and out-of-plane spin signals are unequal. This anisotropic Hanle line shape generally indicates different spin relaxation rates for spins aligned parallel and perpendicular to the plane of the NM channel [9,10]. However, anisotropic spin relaxation in a polycrystalline metallic film has not been observed in the literature and is unexpected, especially being stronger at higher temperatures. Such a temperature dependence of the anisotropy is indicative of a thermoelectric origin. With the help of analytical and numerical thermoelectric transport models, we ascribe the anisotropy in the Hanle measurements to a change in the baseline resistance [14] due to the anisotropy in the Seebeck and Peltier coefficients of the FM. The results evidence how an apparent anisotropic spin precession can develop in an isotropic NM channel, via the coexistence of spin and heat currents and spin-orbit coupling in the FM.

Py/Al NLSVs with transparent interfaces (interface resistance $<10^{-15}\ \Omega\,m^2$) and varying injector-detector separations (L) were prepared on top of a 300-nm-thick SiO_2 layer on a Si substrate. The device preparation is described in detail in the Supplemental Material [15] and follows Refs. [6,13,14]. Figure 1(a) shows an scanning electron microscope (SEM) image of a representative NLSV along with the electrical connections for spin-valve and Hanle measurements. A low frequency (13 Hz) alternating current ($I = 400\ \mu$A) was applied between the injector (Py1) and the left end of the Al channel. The first harmonic response of the corresponding nonlocal signal ($R_{NL} = V_{NL}/I$) was measured between the detector (Py2) and the right end of the Al channel by standard lock-in technique.

The NLSVs were first characterized via spin-valve measurements as shown in Fig. 1(b). An external magnetic field (B_y) was swept along the main axis of the FMs to orient their magnetization in either parallel (P) or antiparallel (AP) configurations, corresponding to distinct levels R_{NL}^{P} and R_{NL}^{AP} in the nonlocal response. From these measurements we extracted the spin accumulation signal in the Al channel, $R_S = R_{NL}^{P} - R_{NL}^{AP}$, and the baseline resistance, $R_B = (R_{NL}^{P} + R_{NL}^{AP})/2$ (which later will be used to interpret the spin precession measurements). The spin accumulation created at the injector junction decays exponentially in the Al channel with a

*K.S.Das@rug.nl

†ivan.veramarun@manchester.ac.uk

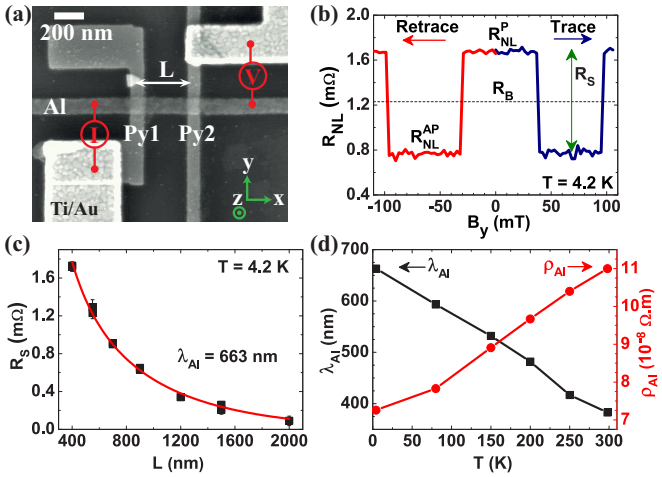

FIG. 1. (a) An SEM image of a representative NLSV along with the electrical connections for spin-valve and Hanle measurements. Py1 and Py2 act as spin injector and detector, respectively, separated by a distance L. (b) Spin-valve measurement on a device with $L = 700$ nm at $T = 4.2$ K. The parallel (R_{NL}^{P}) and antiparallel (R_{NL}^{AP}) states are shown along with the baseline resistance (R_B) and the spin accumulation signal (R_S). (c) Dependence of R_S on L, used to extract the spin relaxation length in Al (λ_{Al}), by fitting the data (black squares) with a spin diffusion model (red line) as described in the text. The error bars correspond to the noise (standard deviation) in the spin-valve curves when quantifying R_{NL}^{P} and R_{NL}^{AP} signals. (d) Temperature dependence of λ_{Al} and the resistivity of the Al channel (ρ_{Al}).

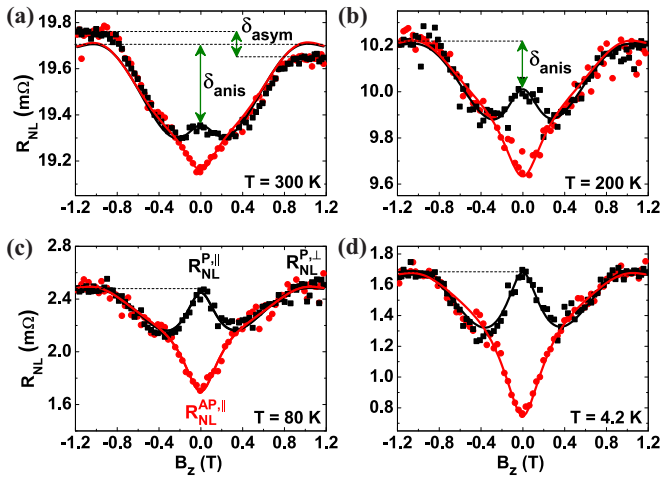

FIG. 2. Hanle measurements in a NLSV with $L = 700$ nm at different temperatures: (a) $T = 300$ K, (b) $T = 200$ K, (c) $T = 80$ K, and (d) $T = 4.2$ K. The initial magnetic configuration of the FM contacts at $B_z = 0$ is in plane and either parallel ($R_{NL}^{P,\parallel}$, black squares) or antiparallel ($R_{NL}^{AP,\parallel}$, red circles), whereas for $|B_z| > 0.9$ T it is out of plane and parallel ($R_{NL}^{P,\perp}$). The anisotropy (δ_{anis}) in the nonlocal signal (R_{NL}) between spins oriented in plane (y) and out of plane (z) is observed at 300 and 200 K, but it is absent at 80 and 4.2 K. The solid lines are fits to the Hanle data (see text).

characteristic spin relaxation length, λ_{Al}. Figure 1(c) shows the dependence of R_S on the injector-detector separation (L), from which λ_{Al} can be extracted using the standard spin diffusion formalism for transparent contacts [16–18]. We extracted λ_{Al} to be 663 nm at 4.2 K and 383 nm at 300 K. A systematic study of the temperature dependence of λ_{Al} revealed its monotonic decrease with increasing T, with an opposite behavior for the resistivity of the channel (ρ_{Al}), as shown in Fig. 1(d). These results are consistent with the Elliott-Yafet spin relaxation mechanism dominated by electron-phonon interaction in bulk metal [8,11,19], in which the spin relaxation length is proportional to the electron mean free path.

Next, we perform Hanle spin precession measurements, in which a perpendicular magnetic field (B_z) induces the spins injected into the Al channel to precess at a Larmor frequency $\omega_L = g\mu_B B_z/\hbar$, where $g \approx 2$ is the g factor in Al, μ_B is the Bohr magneton, and $\hbar$ is the reduced Planck constant. As shown in Figs. 2(a)–2(d), Hanle measurements can be performed with the magnetizations of the FMs initially aligned in plane (at $B_z = 0$) and set either parallel (P) or antiparallel (AP) with respect to each other. The Larmor precession and the resulting spin dephasing, lead to a decrease (increase) in the signal R_{NL} with increasing $|B_z|$ for the P (AP) configuration, eventually intersecting the AP (P) curve for an average spin rotation of $\pi/2$. After the intersection of the P and AP curves, they bend upwards with increasing $|B_z|$ and finally saturate for $|B_z| \geqslant 0.9$ T. This happens because the magnetization of Py starts to rotate out of plane and finally aligns with B_z for $|B_z| \geqslant 0.9$ T. The rotation of Py's magnetization with B_z can be checked from the anisotropic magnetoresistance (AMR) measurements of the Py wire, described in the Supplemental Material [15] and follows Refs. [3,20]. Thus, for $|B_z| \geqslant 0.9$ T, the spins are injected (and detected) in the out-of-plane (z) direction and there should be no precession caused by B_z. For isotropic spin relaxation and parallel orientation of the magnetizations, the signal $R_{NL}^{P,\parallel}$ for spins injected in plane at $B_z = 0$ should be equal to the signal $R_{NL}^{P,\perp}$ when spins are injected out of plane at $|B_z| \geqslant 0.9$ T. We indeed observe that $R_{NL}^{P,\parallel} = R_{NL}^{P,\perp}$ for the Hanle data at 80 and 4.2 K [Figs. 2(c) and 2(d)]. These Hanle data were fitted with an analytical expression obtained by solving the Bloch equation considering spin precession, diffusion, and relaxation for transparent contacts [13,21] and taking into account the out-of-plane rotation of the Py magnetization [3]. From the fitting, we obtained λ_{Al} to be 688 nm at 4.2 K and 544 nm at 80 K, which are comparable to the values obtained from the spin-valve measurements [Fig. 1(d)].

At higher temperatures ($T \geqslant 150$ K), we notice a significant difference between $R_{NL}^{P,\parallel}$ and $R_{NL}^{P,\perp}$, leading to anisotropic Hanle line shapes as shown in Figs. 2(a) and 2(b). Such Hanle line shapes have been hitherto associated with anisotropic spin relaxation [9,10], in which the NM channel has different spin relaxation times for the in-plane and out-of-plane spin directions. For isotropic and polycrystalline metallic films, as is the case for our 50-nm-thick Al channel, the transverse and longitudinal spin relaxation times are expected to be equal [11]. Moreover, by increasing the temperature we expect any anisotropy to decrease due to the thermal disorder in the system. Hence we rule out anisotropic spin relaxation in our system and investigate other causes for the observed

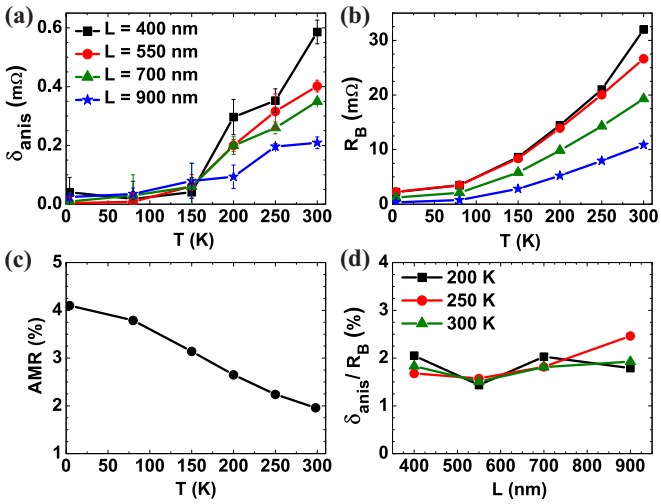

FIG. 3. Temperature (T) dependence of (a) the anisotropy (δ_{anis}) extracted from Hanle measurements for different channel lengths (L), (b) the baseline resistance (R_{B}) extracted from spin-valve measurements, and (c) anisotropic magnetoresistance (AMR) of Py. (d) A constant ratio $\delta_{\text{anis}}/R_{\text{B}} \approx 2\%$ is observed, independent of L and T.

Hanle line shapes. Further checks were performed to rule out (i) the role of interfacial roughness and magnetic impurities by probing the presence of inverted Hanle response [22,23] in the spin-valve measurements at high in-plane fields (B_{y}), (ii) nonlinear effects by measuring higher harmonics and at different current densities, (iii) current inhomogeneity at the contacts, and (iv) frequency dependence. For details of these further checks, see the Supplemental Material [15].

We quantify the anisotropy in the Hanle measurements by the parameter $\delta_{\text{anis}} = R_{\text{NL}}^{\text{P},\perp} - R_{\text{NL}}^{\text{P},\parallel}$, as shown in Figs. 2(a) and 2(b). We note that concurrent to this anisotropy we also observe a smaller asymmetry with the sign of B_{z}, $\delta_{\text{asym}} = R_{\text{NL}}^{\text{P},\perp}(B_{\text{z}} < -0.9\,\text{T}) - R_{\text{NL}}^{\text{P},\perp}(B_{\text{z}} > 0.9\,\text{T})$, as shown in Fig. 2(a). Since $\delta_{\text{asym}} \ll \delta_{\text{anis}}$ we focus the discussion below on the anisotropy (δ_{anis}).

A marked nonlinear increase with temperature is observed on both the anisotropy δ_{anis} (extracted from Hanle measurements) and the baseline resistance R_{B} (obtained from spin-valve measurements) in the measurements summarized in Figs. 3(a) and 3(b). We interpret these observations as an indication for a common thermal origin for both effects. Note that these trends are inconsistent with an effect purely related to spin currents, as λ_{Al} decreases at higher T [Fig. 1(d)]. Furthermore, the trends are also inconsistent with the trivial effect of AMR on local charge currents, because the AMR has also an opposite trend with temperature [Fig. 3(c)]. We remark that the origin of R_{B} in NLSVs has been identified as thermoelectric in nature [14]. It is driven by the interplay of Peltier cooling and heating at the injector junction, in which a charge current across the junction results in a temperature difference, and the Seebeck effect at the detector junction, which acts as a nanoscale thermocouple to electrically detect the nonlocal heat currents. Here, we hypothesize that the anisotropy δ_{anis} is also thermoelectric in nature, in particular given the striking observation of an almost constant ratio $\delta_{\text{anis}}/R_{\text{B}} \approx 2\%$ independent of L and T, as shown in Fig. 3(d).

To further understand the origin of the anisotropy δ_{anis}, we must note that $|B_{\text{z}}|$ modulates the magnetization direction of Py, which together with Al forms thermoelectric junctions. Similarly as the electrical resistance of Py gets modulated due to AMR, we consider here a modulation in the Seebeck (S) and Peltier (Π) coefficients as a function of the angle between the magnetization and the heat current, i.e., anisotropic thermoelectric transport due to spin-orbit interaction in the FM [24–27]. To test this hypothesis, we develop a thermoelectric model to estimate R_{B} in our NLSVs, and relate its corresponding magnetothermoelectric effect to δ_{anis}.

The Peltier effect at the injector junction results in a temperature difference (ΔT), with respect to the reference temperature (T), equal to

$$\Delta T = \dot{Q} R_{\text{th}} = (\Pi_{\text{Al}} - \Pi_{\text{Py}}) I R_{\text{th}}, \tag{1}$$

where $\dot{Q}$ is the rate of Peltier heating for a current (I) from Al into Py, $\Pi_{\text{Al(Py)}}$ is the Peltier coefficient of Al (Py), and R_{th} is the total thermal resistance at the Py/Al junction. In analogy to the standard spin diffusion formalism used to calculate spin resistance R_{S} [16,28], we implement an analytical heat diffusion model that allows us to calculate R_{th} [15,29]. Common to both models, such a resistance is dependent on the corresponding conductivity and the characteristic decay length of the corresponding accumulation. For the thermal model, we consider the thermal conductivity κ and a thermal transfer length L_{T} given by the nonconserved heat current along the metal channel due to the heat flow into the SiO_2/Si substrate [15,29,30], which leads to $L_{\text{T}} \approx 900$ nm in the Al channel at 300 K. The total thermal resistance experienced at the injector junction is $R_{\text{th}} \approx 8.8 \times 10^5$ K/W, which is dominated by the higher κ of the Al channel. From Eq. (1), the temperature difference at the injector was found to be $\Delta T \approx 1.7$ K, which is in good agreement with the temperature profile of the device area as shown in Fig. 4(a) (simulated by three-dimensional finite element modeling, described later in the text). A nonlocal Seebeck signal V_{th} is generated due to ΔT at a distance L from the injector, given by

$$V_{\text{th}} = (S_{\text{Al}} - S_{\text{Py}}) \Delta T e^{-L/L_{\text{T}}}. \tag{2}$$

The modeled thermal signal (V_{th}/I) is shown as a function of L in Fig. 4(b), together with the experimental baseline resistance (R_{B}). The agreement confirms the thermoelectric origin of the latter, with $R_{\text{B}} \approx V_{\text{th}}/I$. The measured first harmonic response shown in Figs. 3 and 4 is in the linear regime accounting only for the Peltier heating/cooling and therefore excludes Joule heating. Without having used any fitting parameters, our analytical model is accurate within a factor of 2 of the experimentally obtained results. This model disregards lateral heat spreading in the narrow channel and hence serves as an upper estimate of R_{B} [15,29,30]. Furthermore, considering the Thomson-Onsager relation $\Pi = ST$ and a linear temperature dependence of the Seebeck coefficient, we predict a nonlinear dependence of R_{B}, which is also substantiated by the measurements in Fig. 3(b).

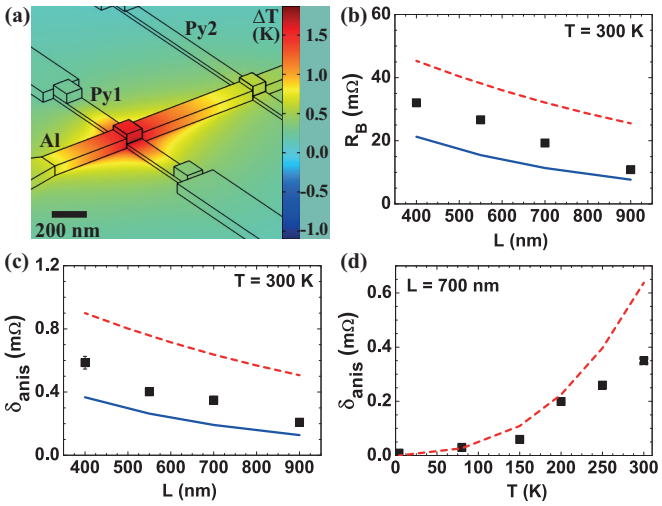

FIG. 4. (a) The temperature difference (ΔT) in the device area, simulated by three-dimensional finite element modeling (3D-FEM), is shown as a color map. Comparison between the measured data (black squares), the analytical model (red dashed lines), and 3D-FEM (blue solid lines) is presented for the dependence of the (b) baseline resistance (R_B) and (c) anisotropy (δ_{anis}) on the channel length (L) at 300 K. (d) Temperature dependence of δ_{anis}, obtained experimentally and through the analytical model, for a fixed channel length of 700 nm.

We address next our central hypothesis that the anisotropy in the Hanle measurements (δ_{anis}) emerges via the anisotropy in the thermoelectric coefficients of Py. To account for these magnetothermoelectric effects [24,26], we relate the isotropic (R_B) and the anisotropic (δ_{anis}) thermoelectric signals, since from Eqs. (1) and (2) and the Thomson-Onsager relation, we find that $V_{th} \propto \Pi_{Py} S_{Py} \propto \Pi_{Py}^2$. This allows us to explain the ratio $\delta_{anis}/R_B \approx 2\%$, observed in Fig. 3(d), by considering an anisotropy in the thermoelectric coefficients of Py (Π_{Py}, S_{Py}) of approximately 1%. This direct extraction of the anisotropy, $\Delta\Pi_{Py}/\Pi_{Py} \approx 1\%$, allows us to successfully model both the channel length (L) and temperature (T) dependence of the thermoelectric signals, as shown in Figs. 4(b)–4(d). Our observation of 1% anisotropic magnetothermopower in Py is in agreement with previous studies on Ni nanowires which put a limit of up to 10% [24,26].

For completeness, we consider a different anisotropic effect: the modulation in the thermal conductivity of Py, and hence on R_{th}, as a consequence of AMR and the Wiedemann-Franz law. Taking the measured AMR $= 2\%$ at room temperature as an upper limit [27], we obtain an anisotropy which is lower by an order of magnitude than the measured one, and therefore cannot account for the observations. The negligible modulation via this effect is understood by the dominant role of the Al channel (which has no AMR) in determining the total R_{th}.

Finally, an accurate three-dimensional finite element model (3D-FEM) was developed incorporating the physics of both the anisotropy of the thermoelectric coefficients and of AMR. It is seen in Figs. 4(b) and 4(c) that the 3D-FEM shows good agreement with the data. A detailed description of the model is included in the Supplemental Material [15]. Having established the thermal origin of the baseline resistance and the anisotropy, we use this 3D-FEM to explore the asymmetry (δ_{asym}) observed in the Hanle measurement at 300 K. A finite component of the heat current in the Py bar at the detector junction flowing along the length of the Al channel, combined with the Py magnetization pointing in the out-of-plane direction, generates a transversal voltage along the main axis of the Py bar due to the the anomalous Nernst effect [25,31]. This transversal voltage gives rise to the asymmetry observed in the Hanle measurements. We successfully account for δ_{asym} by considering an anomalous Nernst coefficient of Py equal to 0.06, a factor of 2 smaller than obtained earlier in Py/Cu spin valves [25].

The magnetothermoelectric effects here described are general phenomena in Hanle experiments. Note that the use of tunnel interfaces in previous studies [3,9,10] enhances the spin signal by about 100 times, but from our thermal model that would only amount to an enhancement of the thermoelectric response by a factor of 1. This allows us to understand why the anisotropic signatures have not been identified in previous studies, as the thermoelectric response would only be a modulation of approximately 1% relative to the spin-dependent Hanle signal in those studies. In this work, with transparent contacts and at room temperature, the spin signals are comparable to the thermoelectric effects, making the latter relevant for correct interpretation of the spin-dependent signals.

We thank J. G. Holstein, H. M. de Roosz, H. Adema, and T. Schouten for their technical assistance. We acknowledge the financial support of the Zernike Institute for Advanced Materials and the Future and Emerging Technologies (FET) programme under FET-Open Grant No. 618083 (CNTQC).

[1] M. Johnson and R. H. Silsbee, Phys. Rev. Lett. **55**, 1790 (1985).
[2] F. J. Jedema, A. T. Filip, and B. J. van Wees, Nature (London) **410**, 345 (2001).
[3] F. J. Jedema, H. B. Heersche, A. T. Filip, J. J. A. Baselmans, and B. J. van Wees, Nature (London) **416**, 713 (2002).
[4] F. J. Jedema, M. S. Nijboer, A. T. Filip, and B. J. van Wees, Phys. Rev. B **67**, 085319 (2003).
[5] S. O. Valenzuela and M. Tinkham, Appl. Phys. Lett. **85**, 5914 (2004).
[6] T. Kimura and Y. Otani, Phys. Rev. Lett. **99**, 196604 (2007).
[7] N. Tombros, C. Jozsa, M. Popinciuc, H. T. Jonkman, and B. J. van Wees, Nature (London) **448**, 571 (2007).
[8] T. Kimura, T. Sato, and Y. Otani, Phys. Rev. Lett. **100**, 066602 (2008).
[9] N. Tombros, S. Tanabe, A. Veligura, C. Jozsa, M. Popinciuc, H. T. Jonkman, and B. J. van Wees, Phys. Rev. Lett. **101**, 046601 (2008).
[10] M. H. D. Guimarães, P. J. Zomer, J. Ingla-Aynés, J. C. Brant, N. Tombros, and B. J. van Wees, Phys. Rev. Lett. **113**, 086602 (2014).

[11] I. Žutić, J. Fabian, and S. Das Sarma, Rev. Mod. Phys. **76**, 323 (2004).
[12] H. Idzuchi, Y. Fukuma, S. Takahashi, S. Maekawa, and Y. Otani, Phys. Rev. B **89**, 081308(R) (2014).
[13] E. Villamor, L. E. Hueso, and F. Casanova, J. Appl. Phys. **117**, 223911 (2015).
[14] F. L. Bakker, A. Slachter, J.-P. Adam, and B. J. van Wees, Phys. Rev. Lett. **105**, 136601 (2010).
[15] See Supplemental Material at http://link.aps.org/supplemental/10.1103/PhysRevB.94.180403 for details on device fabrication, AMR measurements of Py, Hanle fitting, the analytical heat diffusion model, the 3D-FEM and checks for inverted Hanle, higher harmonics detection, and injection current dependence.
[16] S. Takahashi and S. Maekawa, Phys. Rev. B **67**, 052409 (2003).
[17] T. Valet and A. Fert, Phys. Rev. B **48**, 7099 (1993).
[18] G. Schmidt, D. Ferrand, L. W. Molenkamp, A. T. Filip, and B. J. van Wees, Phys. Rev. B **62**, R4790(R) (2000).
[19] G. Mihajlović, J. E. Pearson, S. D. Bader, and A. Hoffmann, Phys. Rev. Lett. **104**, 237202 (2010).
[20] T. G. S. M. Rijks, R. Coehoorn, M. J. M. de Jong, and W. J. M. de Jonge, Phys. Rev. B **51**, 283 (1995).
[21] Y. Fukuma, L. Wang, H. Idzuchi, S. Takahashi, S. Maekawa, and Y. Otani, Nat. Mater. **10**, 527 (2011).
[22] S. P. Dash, S. Sharma, J. C. Le Breton, J. Peiro, H. Jaffrés, J.-M. George, A. Lemaître, and R. Jansen, Phys. Rev. B **84**, 054410 (2011).
[23] G. Mihajlović, S. I. Erlingsson, K. Výborný, J. E. Pearson, S. D. Bader, and A. Hoffmann, Phys. Rev. B **84**, 132407 (2011).
[24] J.-E. Wegrowe, Q. A. Nguyen, M. Al-Barki, J.-F. Dayen, T. L. Wade, and H.-J. Drouhin, Phys. Rev. B **73**, 134422 (2006).
[25] A. Slachter, F. L. Bakker, and B. J. van Wees, Phys. Rev. B **84**, 020412(R) (2011).
[26] R. Mitdank, M. Handwerg, C. Steinweg, W. Töllner, M. Daub, K. Nielsch, and S. F. Fischer, J. Appl. Phys. **111**, 104320 (2012).
[27] J. Kimling, J. Gooth, and K. Nielsch, Phys. Rev. B **87**, 094409 (2013).
[28] T. Maassen, I. J. Vera-Marun, M. H. D. Guimarães, and B. J. van Wees, Phys. Rev. B **86**, 235408 (2012).
[29] I. J. Vera-Marun, J. J. van den Berg, F. K. Dejene, and B. J. van Wees, Nat. Commun. **7**, 11525 (2016).
[30] M.-H. Bae, Z.-Y. Ong, D. Estrada, and E. Pop, Nano Lett. **10**, 4787 (2010).
[31] S. Hu and T. Kimura, Phys. Rev. B **87**, 014424 (2013).